Giant universal conductance fluctuations in the antiferromagnetic topological insulator MnBi2Te4

Michael Wissmann, Joseph Dufouleur, Louis Veyrat, Anna Isaeva, Laurent Vila, Bernd Büchner, Romain Giraud

▶ **To cite this version:**

Michael Wissmann, Joseph Dufouleur, Louis Veyrat, Anna Isaeva, Laurent Vila, et al.. Giant universal conductance fluctuations in the antiferromagnetic topological insulator MnBi2Te4. 2025. ⟨hal-04910693⟩

HAL Id: hal-04910693

https://hal.univ-grenoble-alpes.fr/hal-04910693v1

Preprint submitted on 24 Jan 2025

HAL is a multi-disciplinary open access archive for the deposit and dissemination of scientific research documents, whether they are published or not. The documents may come from teaching and research institutions in France or abroad, or from public or private research centers.

L'archive ouverte pluridisciplinaire **HAL**, est destinée au dépôt et à la diffusion de documents scientifiques de niveau recherche, publiés ou non, émanant des établissements d'enseignement et de recherche français ou étrangers, des laboratoires publics ou privés.

Distributed under a Creative Commons CC BY 4.0 - Attribution - International License

Giant universal conductance fluctuations in the antiferromagnetic topological insulator $MnBi_2Te_4$

Michael Wissmann[1,2,3], Joseph Dufouleur[1], Louis Veyrat[1,5], Anna Isaeva[1,4], Laurent Vila[3], Bernd Büchner[1,2], and Romain Giraud[1,3*]

[1]*Leibniz Institute for Solid State and Materials Research IFW Dresden, 01069 Dresden, Germany*

[2]*Institute of Solid State Physics, TU Dresden, 01069 Dresden, Germany*

[3]*Université Grenoble Alpes, CNRS, CEA, Spintec, F-38000 Grenoble, France*

[4]*Institute of Physics, University of Amsterdam, 1098 XH Amsterdam, The Netherlands and*

[5]*Laboratoire National des Champs Magnetiques Intenses LNCMI, CNRS-INSA-UJF-UPS, UPR3228, F-31400 Toulouse, France*

(Dated: January 29, 2025)

Abstract

The study of quantum coherent transport in mesoscopic Hall bars fabricated from exfoliated $MnBi_2Te_4$ single-crystals reveals giant-amplitude universal conductance fluctuations, related to the longest phase-coherence length L_φ observed in a mesoscopic magnet, as well as the weak decoherence in magnetic topological insulators. By comparing different magnetic configurations, we identify the contributions to dephasing due to structural disorder (magnetic flux) or magnetism (local magnetic disorder or domain-related Berry phase). These results show the potential of magnetic topological insulators to realize quantum interferometers based on dephasing by magnetism.

The magnetization dynamics in nanostructures is a key limiting factor to quantum interference effects evidenced by charge transport measurements, since inelastic scattering in a magnet can severely reduce the decoherence time τ_φ and related phase-coherence length L_φ. Both collective excitations (magnons) and locally-fluctuating magnetic moments usually destroy quantum coherence, so that quantum corrections to the conductance are vanishingly small in ferromagnetic-metal nanostructures ($L_\varphi < 30$ nm at $T = 30$ mK) and the temperature dependence of decoherence is stronger than in normal metals [1–5]. A significant increase of L_φ at very low temperature, by about an order of magnitude, was evidenced in nanostructures of single-crystalline ferromagnets with a large anisotropy [6–8], a favorable situation to reduce magnetic fluctuations at very low temperatures. In this case, an additional contribution to dephasing related to magnetism was evidenced, as induced by local magnetic textures [7] or by the Berry phase associated to the electronic band structure of magnetic domains [9]. To date, such a situation to realize a mesoscopic magnet remains scarce however, and decoherence remains an important limitation above 1K (even in diluted ferromagnetic semiconductors [7]).

Recently, the antiferromagnetic topological insulator $MnBi_2Te_4$ has gained increasing attention as a potential platform to realize exotic topological phases controlled by magnetic order [10], such as the quantum anomalous Hall or the axion insulators [11, 12], by combining magnetism and non-trivial band-structure topology. Similarly to diluted ferromagnetic semiconductors, intrinsic magnetic topological insulators are crystalline magnets with a large uniaxial anisotropy. Moreover, their magnetization is more homogenous than that of diluted magnets, and their electronic band structure can have some rather large topological gaps.

* romain.giraud@cea.fr

This situation is favorable to quantum interference phenomena and, indeed, universal conductance fluctuations (UCF) related to magnetism were evidenced in Hall bars of ultra-thin $MnBi_2Te_4$ grown by molecular-beam epitaxy (MBE) [13], with a rather small amplitude of UCF for long conductors, in the $10^{-2}e^2/h$ range Contrary to defect-free bulk single crystals, such MBE films have some local structural disorder (twin domains, local stacking faults or secondary MnTe layers), intrinsic to the MBE growth by islands, with a short correlation length of domains of about or smaller than 200 nm [13, 14]. Even in the absence of extended defects (and for well-textured islands), the rather high density of grain boundaries favors the formation of local non-colinear magnetic textures or domain walls, some of which (loose spins) being responsible for enhanced decoherence.

In this work, we evidence the giant-amplitude universal conductance fluctuations in micron-size nanostructures patterned from exfoliated high-quality $MnBi_2Te_4$ single crystals, with an exceptionally-large amplitude for a mesoscopic magnet. Such reproducible magneto-fingerprints are clearly visible up to 40 K, a direct signature of the limited decoherence in magnetic topological insulators. A careful study of self averaging (length and width dependence of the conductance variance) and of the UCF correlation field reveals that the rather large phase coherence length L_φ, with $L_\varphi \approx 300$ nm at $T = 50$ mK, has only a small decrease at higher temperatures ($L_\varphi \approx 100$ nm at $T = 5$ K), contrary to previous results obtained with (Ga,Mn)As nanostructures. Furthermore, the nature of dephasing is clarified by considering the UCF evolution for different magnetic states, under appropriate orientation of the applied magnetic field, within the sample plane or perpendicular to it. In particular, we identify the two different contributions related to magnetism, that is, the dephasing by static domain walls and that induced by the band-structure related Berry phase in magnetic domains. Remarkably, the correlation field of UCF induced by magnetic dephasing has nearly no temperature dependence in both the colinear and the canted antiferromagnetic states, which could be related to the slow temperature dependence of the spin relaxation length in the long-range magnetic order regime. For all field orientations, the magnetization is uniformed and constant at large magnetic fields, so that magnetism does not contribute to dephasing anymore for $B > 10$ T. In this saturated-magnetization regime, UCF are determined by structural disorder only, as due to the standard flux-trap dephasing associated to closed coherent paths (loops). A similar evolution is seen in temperature, with a vanishing contribution of magnetism to dephasing above the long-range

ordering temperature ($T_N \approx 24$K).

Mesoscopic Hall bars of monocristalline $MnBi_2Te_4$ were obtained by the lateral patterning of thin flakes exfoliated from high-quality single crystals, with a thickness t smaller than about 100 nm. After exfoliation, an ultra-thin TiOx hard mask was prepared by electron-beam lithography, metal evaporation and oxidation, and then used to mill a nano-Hall bar by using an Argon plasma. Ohmic contacts were finally prepared by electron-beam lithography and metal evaporation. In order to evidence the influence of the sample planar geometry on self-averaging, the universal conductance fluctuations were investigated in two devices with a different cross-section (with a width $W = 100$ nm and $W = 500$ nm, and a thickness $t = 110$ nm and $t = 55$ nm, respectively for S1 and S2), each studied with three segments of different lengthes (ranging from 200 nm to 3.5 µm). The samples were mount onto the cold finger on an Oxford MX400 ^{3}He/^{4}He dilution refrigerator, inserted into the bore of a 15 T magnet, and magneto-transport measurements were performed by using low-noise lock-in amplifiers.

We first focus on the evidence of giant-amplitude UCF by applying a magnetic field perpendicular to the sample plane (out-of-plane, OOP configuration), as observed in the narrower Hall bar shown in Fig. 1a) [similar results were obtained with the wider Hall bar, and are included in the scaling analysis of Fig. 4c)]. As seen in Fig. 1b), the magneto-conductance measured at $T = 1$ K shows the expected evolution of the classical conductance with the magnetic state, with a plateau in the antiferromagnetic (AFM) regime, then a jump at the spin-flop transition at $B_\perp \approx= 3$ T, followed by the continuous rotation in the canted-AFM regime, and finally a slope change at the saturation field above which the magnetization is uniform and aligned along the applied field (denoted F, though it is not a ferromagnetic phase by itself). In addition, there is a clear contribution of quantum interference to the magneto-conductance, for all three lengthes of the mesoscopic conductors ($L_{14} = 3500$ nm, $L_{23} = 1700$ nm, $L_{56} = 200$ nm), with an increasing amplitude of universal conductance fluctuations for a shorter conductor length, as expected for a mesoscopic conductor in the self-averaging limit ($L_\varphi < L$). After removing the classical background, the quantum magneto-fingerprint is best seen in Fig. 1c), with three different behaviors for the three different magnetic states. At low field in the AFM regime, reproducible UCF traces and retraces are observed, after substraction of a hysteresis due to the classical magneto-conductance background. A similar reversible behavior is found in the saturated regime (F)

at high magnetic fields, for both the quantum interference and the classical conductance. In the canted-AFM regime however, the UCF show a clear hysteresis, with visible phase shifts but also sudden changes in the conductance that are not due to the classical magneto-conductance (since the magnetization rotates continuously in this regime) and vary from segment to segment.

To better understand the nature of dephasing, the UCF are investigated in two different configurations of the applied magnetic field, either perpendicular to (OOP) or within (IP) the sample plane. The evolution of the micromagnetic state is different for OOP and IP configurations. As seen in Fig. 2a) from the classical magneto-conductance background, the in-plane magnetic field induces directly a continuous rotation of a canted-AFM state in magnetic domains, with no spin-flop transition, and gives little driving force on existing domain walls after a first magnetization curve (which corresponds to minor-loop cycling in the OOP configuration). Whereas the UCF amplitude itself is not changed for different magnetic states (that is, decoherence does not depend on the applied field), the UCF correlation field B_C, which is a direct signature of dephasing, varies at the transition between AFM to c-AFM and between c-AFM to F (see Fig. 2b,c). This is summarized in Fig. 3a), which shows that faster UCF occur in both the AFM and c-AFM states (smaller B_C), as compared to the uniform magnetization F state. Moreover, these faster UCF have nearly no temperature dependence of their correlation field, as expected for spin dephasing by magnetism. On the contrary, B_C in the high-field F state is only due to structural disorder, and it depends on a geometric effect revealed by the comparison of the results obtained in both IP and OOP configurations (Fig. 3b). In this case, the value of B_C is roughly given by the largest coherent loop, of size $L_\varphi < L \times W$ (OOP) or $t \times W$ (IP). This difference is clearly seen in Fig. 3a), and the ratio B_C^{OOP}/B_C^{IP} equals L_φ/t, which gives access to a rough estimation of $L_\varphi \approx 300$ nm at $T = 1$ K.

A thourough analysis can be made further by considering the conductance variance $\mathrm{var}G = \delta G_{rms}^2$, its scaling law with the sample dimensions (width W and length L) and its temperature dependence. This is shown in Fig. 4, first by considering the temperature dependence of δG_{rms} for the long conductor $L_{14} = 3500$ nm, with the condition $L_{14} > L_\varphi(T)$ valid over the full temperature range studied. As seen in Fig. 4a), the UCF in the F state show the typical behavior of quantum interference induced by structural disorder only. Upon increasing temperature, the behavior both the UCF amplitude (decrease) and the correlation

field (increase) is directly related to the decrease of L_φ with temperature. To give a more quantitative description, the nature of dephasing by structural disorder needs to be clarified. Since $MnBi_2Te_4$ can be considered as a dirty metal, the thermal length $L_T = \sqrt{\hbar D/k_B T}$ (dephasing due to elastic scattering) must be compared to the phase-coherence length L_φ, limited by inelastic scattering. For $MnBi_2Te_4$, with a carrier density $n \approx 10^{19}\text{cm}^{-3}$ and a resistivity $\rho \approx 200\Omega\text{cm}$, we find $L_T \approx 350$ nm and $L_T \approx 550$ nm, at $T = 1$ K, for bulk and topological surface states, respectively. These values are comparable to or larger than those of L_φ inferred from the analysis above. For a 2D system and for $L_\varphi < L_T$, the conductance variance depends on the conductor aspect ratio and $\delta G_{rms} \approx \sqrt{W/L} \times L_\varphi/L$ [15], as shown in Fig. 4b). Considering the data obtained for the two samples with different aspect ratios, this scaling analysis gives a value $L_\varphi \approx 300$ nm at $T = 50$ mK, a similar value to that inferred from the correlation-field analysis at $T = 1$ K. This very slow temperature dependence of L_φ results in the slow evolution of δG_{rms} with temperature (Fig. 4c), which confirms the reduced decoherence in magnetic topological insulators as compared to the case of diluted ferromagnetic semiconductors such as (Ga,Mn)As, for which a stronger temperature dependence was found, with $L_\varphi \approx 30$ nm at $T = 1$ K [7].

In conclusion, our results show the rather weak decoherence in a mesoscopic magnet achieved with a magnetic topological insulator, with a rather long phase coherence length being more robust in temperature as compared to the case of diluted ferromagnetic insulators. Still, the origin of this specific behavior found in single-crystalline $MnBi_2Te_4$ nanostructures needs to be clarified (bulk states or topological surface sates). Some more specific studies could shed some new light on the exact nature of quasiparticles responsible for quantum interference in IMTIs (e.g., by studying the thickness or electrical-gate dependence, or by considering other geometries such as a planar Aharonov-Bohm ring).

ACKNOWLEDGMENTS

This work was supported by the European Union's H2020 FET Proactive project TOCHA (No. 824140), as well as by the CNRS International Research Project "CITRON".

[1] K. Hong and N. Giordano, Approach to mesoscopic magnetic measurements, Phys. Rev. B **51**, 9855 (1995).

[2] M. Aprili, J. Lesueur, L. Dumoulin, and P. Nédellec, Weak localization and electron-electron interaction in percolating nickel films, Solid State Communications **102**, 41 (1997).

[3] S. Kasai, E. Saitoh, and H. Miyajima, Quantum transport properties in ferromagnetic nanorings at low temperature, Journal of Applied Physics **93**, 8427 (2003), https://pubs.aip.org/aip/jap/article-pdf/93/10/8427/10624626/8427_1_online.pdf.

[4] S. Lee, A. Trionfi, and D. Natelson, Quantum coherence in a ferromagnetic metal: Time-dependent conductance fluctuations, Phys. Rev. B **70**, 212407 (2004).

[5] Y. G. Wei, X. Y. Liu, L. Y. Zhang, and D. Davidović, Mesoscopic resistance fluctuations in cobalt nanoparticles, Phys. Rev. Lett. **96**, 146803 (2006).

[6] K. Wagner, D. Neumaier, M. Reinwald, W. Wegscheider, and D. Weiss, Dephasing in (ga,mn)as nanowires and rings, Phys. Rev. Lett. **97**, 056803 (2006).

[7] L. Vila, R. Giraud, L. Thevenard, A. Lemaître, F. Pierre, J. Dufouleur, D. Mailly, B. Barbara, and G. Faini, Universal conductance fluctuations in epitaxial GaMnAs ferromagnets: Dephasing by structural and spin disorder, Physical Review Letters **98**, 027204 (2007).

[8] D. Neumaier, K. Wagner, S. Geißler, U. Wurstbauer, J. Sadowski, W. Wegscheider, and D. Weiss, Weak localization in ferromagnetic (Ga,Mn)As nanostructures, Physical Review Letters **99**, 116803 (2007).

[9] M. Granada, D. Lucot, R. Giraud, A. Lemaître, C. Ulysse, X. Waintal, and G. Faini, Direct probing of band-structure Berry phase in diluted magnetic semiconductors, Physical Review B - Condensed Matter and Materials Physics **91**, 235203 (2015).

[10] J. Li, Y. Li, S. Du, Z. Wang, B. L. Gu, S. C. Zhang, K. He, W. Duan, and Y. Xu, Intrinsic magnetic topological insulators in van der Waals layered MnBi2Te4-family materials, Science Advances **5**, eaaw5685 (2019), arXiv:1808.08608.

[11] Y. Deng, Y. Yu, M. Z. Shi, Z. Guo, Z. Xu, J. Wang, X. H. Chen, and Y. Zhang, Quantum anomalous Hall effect in intrinsic magnetic topological insulator MnBi2Te4, Science **367**, 895 (2020).

[12] C. Liu, Y. Wang, H. Li, Y. Wu, Y. Li, J. Li, K. He, Y. Xu, J. Zhang, and Y. Wang, Robust

axion insulator and Chern insulator phases in a two-dimensional antiferromagnetic topological insulator, Nature Materials **19**, 522 (2020).

[13] M. P. Andersen, E. Mikheev, I. T. Rosen, L. Tai, P. Zhang, K. L. Wang, M. A. Kastner, and D. Goldhaber-Gordon, Universal Conductance Fluctuations in a MnBi2Te4 Thin Film, Nano Letters 10.1021/ACS.NANOLETT.3C02932/ASSET/IMAGES/LARGE/NL3C02932$_0$005.$JPEG$ (2023), arXiv:2308.01183.

[14] P. Kagerer, C. I. Fornari, S. Buchberger, S. L. Morelhão, R. C. Vidal, A. Tcakaev, V. Zabolotnyy, E. Weschke, V. Hinkov, M. Kamp, B. Büchner, A. Isaeva, H. Bentmann, and F. Reinert, Molecular beam epitaxy of antiferromagnetic (mnbi2te4)(bi2te3) thin films on baf2 (111), Journal of Applied Physics **128**, 135303 (2020), https://pubs.aip.org/aip/jap/article-pdf/doi/10.1063/5.0025933/15255507/135303_1_online.pdf.

[15] P. A. Lee, A. D. Stone, and H. Fukuyama, Universal conductance fluctuations in metals: Effects of finite temperature, interactions, and magnetic field, Physical Review B **35**, 1039 (1987).

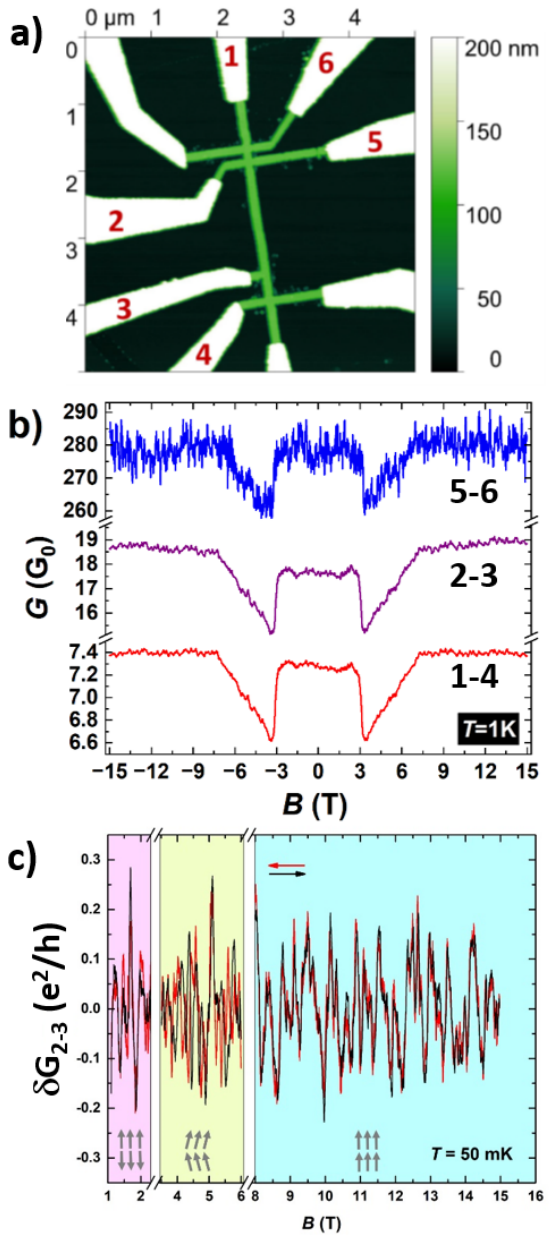

FIG. 1: **a**), AFM image of a $MnBi_2Te_4$ mesoscopic Hall bar patterned from a 100nm-thick exfoliated flake, with TiAu ohmic contacts; **b**), Magneto-conductance at $T = 1$ K measured for three different lengthes ($L_{14} = 3500$ nm, $L_{23} = 1700$ nm, $L_{56} = 200$ nm), with a magnetic field $B_\perp$ applied perpendicular to the sample plane (out-of-plane OOP configuration); **c**), Universal conductance fluctuations δG_{2-3}, after substraction of the classical magneto-conductance, measured at $T = 50$ mK for three different magnetic states (antiferromagnet - AFM, canted antiferromagnet - c-AFM, and saturated magnetization - F).

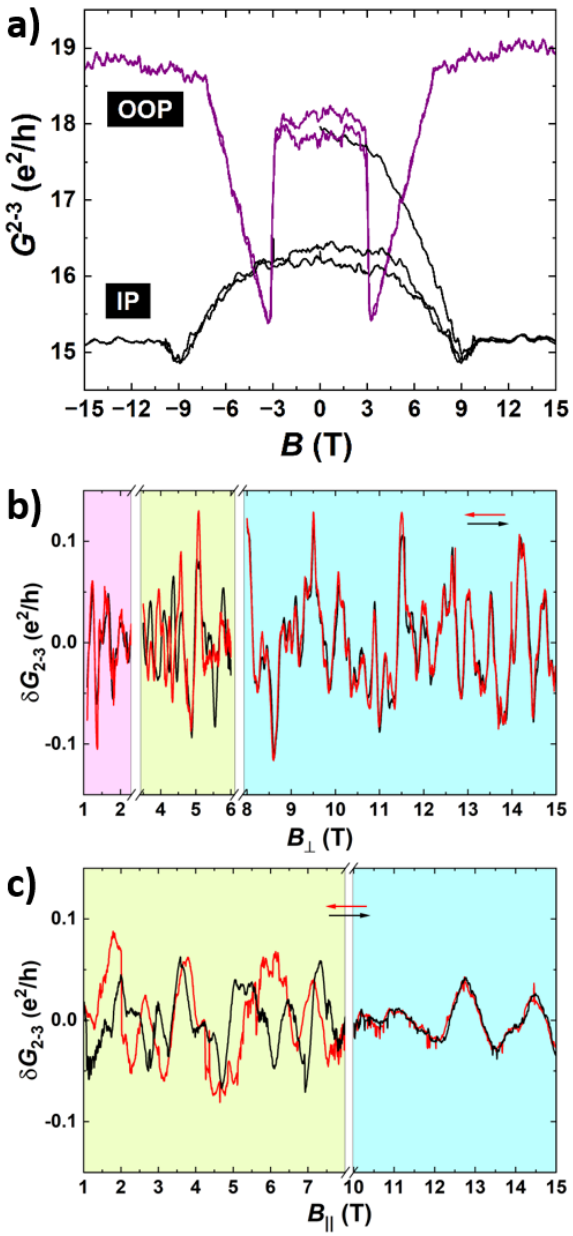

FIG. 2: **a**), Magneto-conductance $G_{2-3}(B)$ measured at $T = 1$ K in two different configurations of the applied magnetic field, either perpendicular to (OOP) or within (IP) the sample plane. In the IP configuration, the sub-layer magnetization rotates continuously away from the anisotropy axis and fully aligns along the applied magnetic field above the saturation field $B_{IP}^{sat} \approx 10$ T; **b,c**), Universal conductance fluctuations δG_{2-3}, after substraction of the classical magneto-conductance, measured at $T = 1$ K in the different magnetic states (AFM, c-AFM, F), for the OOP (b) or IP (c) configuration.

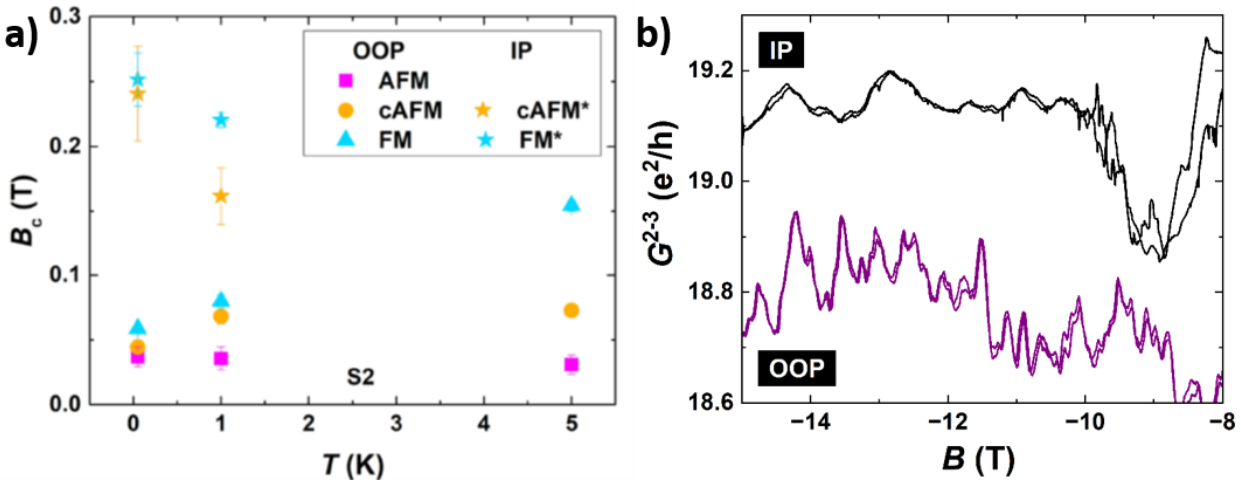

FIG. 3: **a**), Temperature dependence of the correlation field B_C, measured from $G_{2-3}(B)$ traces for different magnetic states, and two configurations of the applied magnetic field (IP and OOP); **b**), Comparison of the magneto-conductance $G_{2-3}(B)$ traces measured at $T = 1$ K in the OOP and IP configurations in the homogenous magnetization regime (F), with an applied magnetic field B larger than the saturation fields $B_{IP}^{sat} > B_{OOP}^{sat}$.

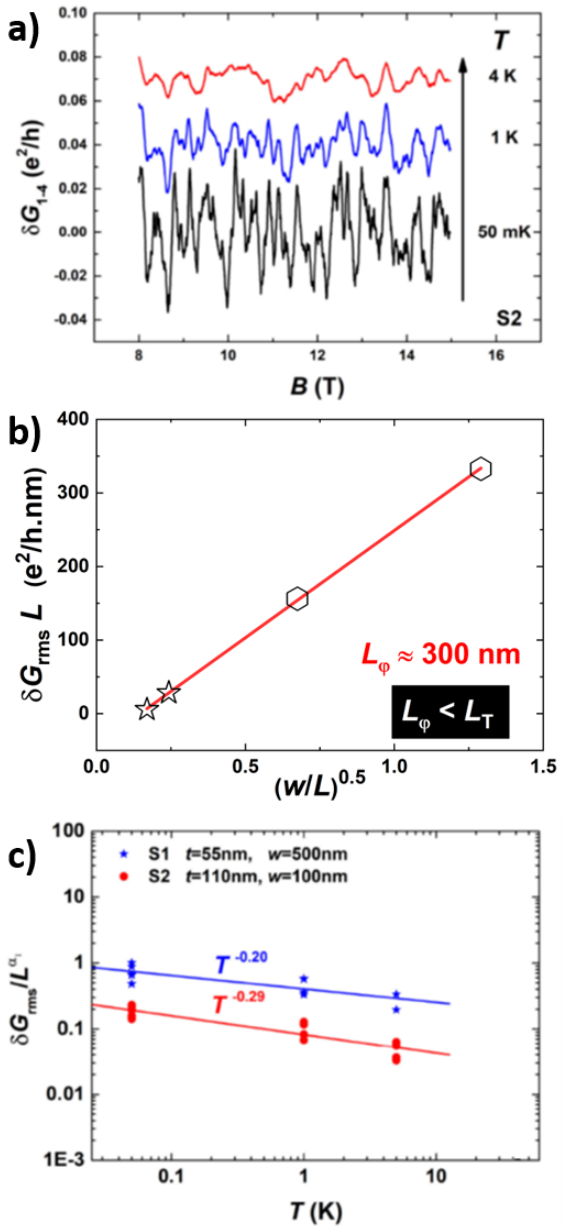

FIG. 4: **a**), Temperature dependence of the universal conductance fluctuations δG_{1-4}, measured with the long conductor in the self-averaging regime ($L_\varphi < L_{1-4}$); **b**), Scaling-law dependence of δG_{rms} with the conductor length L and width W, as measured at $T = 50$ mK from two mesoscopic Hall bars with a different aspect ratio (open hexagons for S1, open stars for S2); **c**), Slow temperature dependence of the UCF amplitude δG_{rms}, in this scaling-law regime for the length dependence of δG_{rms} (quasi-2D quantum coherent regime, with $L_\varphi > L_T > t$).